

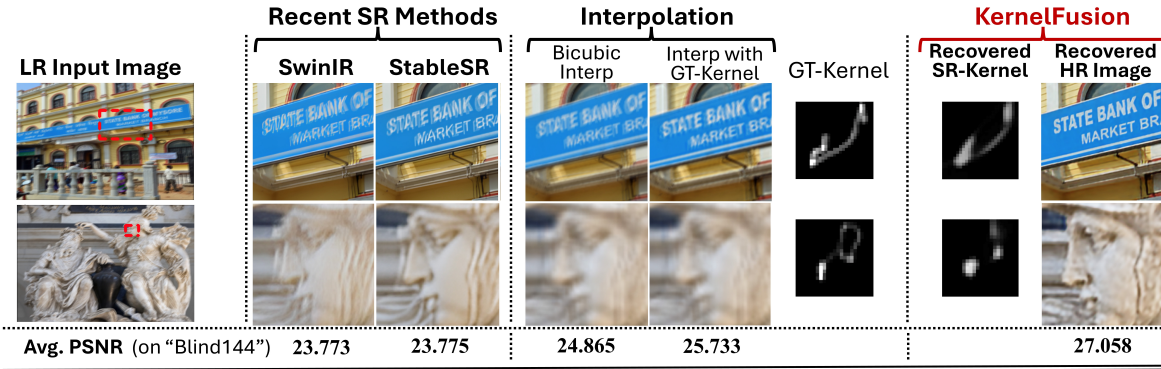
KernelFusion: Assumption-Free Blind Super-Resolution via Patch Diffusion

Oliver Heinimann^{1*} Assaf Shocher^{2*} Tal Zimbalist¹ Michal Irani¹

¹Weizmann Institute of Science

²NVIDIA Research

(a) Current SR methods fail when downscaling kernels are complex (non-Gaussian) :



(b) Existing Kernel estimation methods cannot recover complex SR-Kernels:

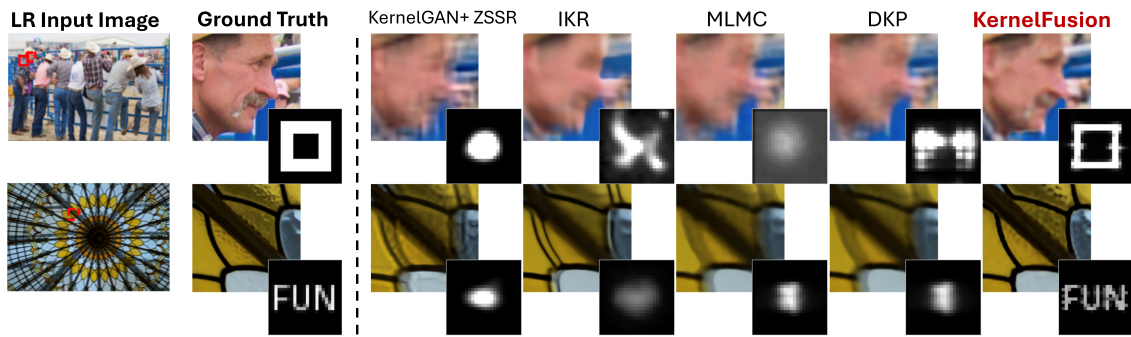


Figure 1. **The importance of an accurate SR-Kernel.** (A) SotA SR-methods fail on complex downscaling kernels outside their training distribution, performing even worse than interpolation on such kernels. (B) Existing SR-kernel estimation methods cannot handle complex downscaling kernels. KernelFusion is the only method capable of estimating arbitrarily challenging SR-kernels.

Abstract

Traditional super-resolution (SR) methods assume an “ideal” downscaling SR-kernel (e.g., bicubic downscaling) between the high-resolution (HR) image and the low-resolution (LR) image. Such methods fail once the LR images are generated differently. Current blind-SR methods aim to remove this assumption, but are still fundamentally restricted to rather simplistic downscaling SR-kernels (e.g., anisotropic Gaussian kernels), and fail on more complex (out of distribution) downscaling degradations. However, using the correct SR-kernel is often more important than using a sophisticated SR algorithm. In “KernelFusion” we introduce a zero-shot diffusion-based method that makes no assumptions about the kernel. Our method recovers the unique image-specific SR-kernel directly from the LR input image, while simultaneously recovering its corresponding HR image. KernelFusion exploits the principle that the

correct SR-kernel is the one that maximizes patch similarity across different scales of the LR image. We first train an image-specific patch-based diffusion model on the single LR input image, capturing its unique internal patch statistics. We then reconstruct a larger HR image with the same learned patch distribution, while simultaneously recovering the correct downscaling SR-kernel that maintains this cross-scale relation between the HR and LR images. Empirical results show that KernelFusion vastly outperforms all SR baselines on complex downscaling degradations, where existing SotA Blind-SR methods fail miserably. By breaking free from predefined kernel assumptions, KernelFusion pushes Blind-SR into a new assumption-free paradigm, handling downscaling kernels previously thought impossible.

*Equal contribution

1. Introduction

Super-resolution (SR) is an inverse problem of recovering a high-resolution (HR) image from its low-resolution (LR) counterpart, given by

$$I_{LR} = (I_{HR} * k_s) \downarrow_s, \quad (1)$$

where k_s is the downscaling kernel (also known as SR kernel) and \downarrow_s denotes subsampling by a scale factor s . Traditional SR methods have achieved impressive results [6, 19, 23, 25, 35, 62, 63] under the assumption that k_s is a global, known kernel (e.g. bicubic with antialiasing), but this is rarely the case. The SR-kernel tends to be *image-specific*; it is affected not only by sensor optics, but also by camera motion, subtle hand movements, and other factors. Evidently, these methods perform poorly in any scenario other than synthetic data specifically created using the assumed kernel. In fact, it was shown [7, 22], that the *accuracy of the SR-kernel is often more critical for obtaining good SR*, than the image prior or the choice of SR algorithm used.

Blind-SR methods have emerged to address this limitation. Some approaches aim to explicitly estimate the unknown kernel (e.g., [3, 31, 54]), whereas others represent the SR-kernel implicitly [2, 10, 14, 20, 29], or aim to design networks that are robust to kernel variations (e.g., [24, 26, 28, 30, 46, 50]). However, existing Blind-SR methods are fundamentally limited: They can only super-resolve well LR images which were downsampled by simple, low-pass-filter kernels (e.g., (an)isotropic Gaussians), and fail on more complex downscaling kernels, which are outside their training distribution. In fact, *for LR images obtained by non-Gaussian downscaling kernels, SOTA Blind-SR methods perform worse than simple interpolation.* (see Fig. 1a and Sec. 3).

In “KernelFusion” we introduce a zero-shot diffusion-based method that makes no assumptions (explicitly or implicitly) about the downscaling kernel. Our method recovers the unique image-specific SR-kernel directly from the LR input image, while *simultaneously* recovering its corresponding HR image. KernelFusion exploits the principle (presented by [31] and used in [3]), that the correct SR-kernel is the one that also maximizes patch similarity across different scales of the LR image. More specifically, we first train an *image-specific* patch-based diffusion model on the single LR input image, capturing its unique internal patch statistics. We then freeze the patch-diffusion model, and use it to reconstruct a larger HR image with the same learned patch distribution. After each HR diffusion denoising step, we iteratively recover the estimated HR image while simultaneously estimating the downscaling SR-kernel that maintains this cross-scale relation between the HR and LR images. Empirical results show that KernelFusion vastly outperforms all SR baselines on complex downscaling degra-

dations, where existing SotA Blind-SR methods fail miserably.

The success of KernelFusion in handling complex downscaling kernels (where all previous SR methods fail), stems from the following critical design choices:

1. Being a zero-shot estimation method which trains *internally* on the LR input image only, KernelFusion is not bound by any external training distribution, hence can handle any type of downscaling kernel. There is no notion of “out-of-distribution” kernels, which *externally-trained* Blind-SR methods suffer from (see Fig. 1a).
2. Previous zero-shot SR-kernel methods [3, 31] estimated the kernel only. They require a separate independent SR algorithm to super-resolve the LR image with their recovered kernel (e.g., using ZSSR [39] or SRMD [57], which can receive a user-specified kernel). Such a 2-step process suffers from accumulated errors and inconsistencies between the estimated kernel and the estimated HR image. In contrast, KernelFusion *simultaneously* estimates both the SR-kernel and the corresponding HR image *in a consistent manner*.
3. The explicit kernel estimation methods of [2, 3, 54, 56] seem to recover well only specific types of kernels (Gaussians and motion lines). We suspect that this limitation stems from the implicit-bias of the CNN and MLP architectures, which tend to produce smooth outputs (as also observed in [44]). In contrast, the kernel-estimation component in KernelFusion employs an *Implicit Neural Representation* (INR) architecture, which allows for the recovery of complex *non-smooth* downscaling SR-kernels (see Fig. 1).

By breaking free from predefined kernel assumptions, KernelFusion pushes Blind-SR into a new, assumption-free paradigm — handling out-of-distribution (non-Gaussian) downscaling kernels, which were previously out of reach.

Our contributions are therefore as follows:

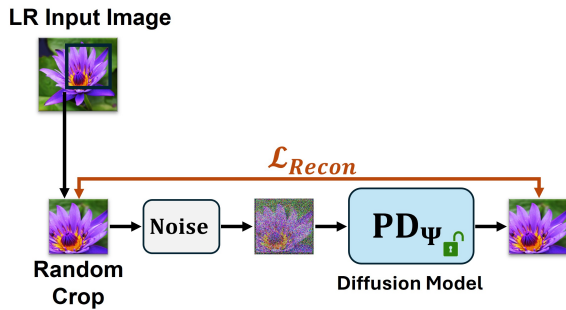
- *KernelFusion* is the first deep Blind-SR method capable of recovering arbitrary downscaling SR-kernels.
- *KernelFusion* obtains state-of-the-art SR results on challenging downscaling degradations, where leading SR methods fail.

2. Related Work

We start by describing three main types of Blind-SR [27]. Finally, we review diffusion models and their use for inverse problems, which is related to our method.

Blind-SR by training on synthetic degradations: One type of Blind-SR involves training on data with synthetic degradations out of a predefined distribution of degradations. They can be applied to data close to that distribution and achieve visually pleasing results. Among them are SwinIR [24], Real-ESRGAN [48] and many more [5, 17, 26, 28, 43, 52, 53, 55, 60, 61]. These methods are inherently restricted by their training distribution, thus fail

Phase 1: Patch Diffusion (PD) Training



Phase 2: Blind Super Resolution

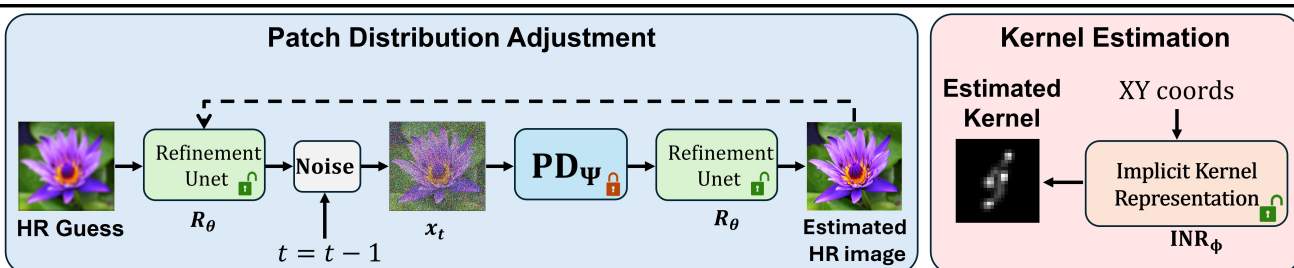
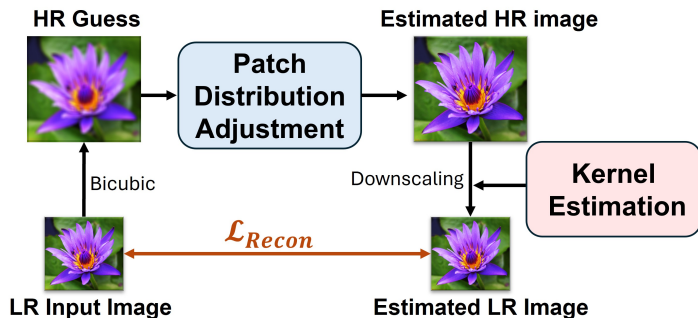


Figure 2. **Method Overview.** Our approach consists of 2 stages: **Phase 1:** We train a diffusion model (PD) to learn the patch distribution of a single image. **Phase 2:** We perform blind SR and kernel estimation simultaneously. In particular, we use the trained PD to shift the HR guess toward the patch distribution of the LR input. A refinement U-Net and an implicit kernel representation model are trained jointly under a consistency loss, ensuring that convolving the estimated HR image with the learned kernel reproduces the original LR image.

on LR images generated by out-of-distribution downscaling kernels (e.g., non-Gaussian kernels).

Blind-SR with latent kernel representation: other methods represent degradations by a latent features vector. These methods perform SR and refinement of the degradation features, often based on alternating SR and latent kernel estimation as was first shown by IKC [10], later improved by unfolding this alternation with DAN [14, 29] and many more [20, 28, 42, 59]. The kernel representation is data-driven, hence also based on the synthetic degradations used at training. This makes them fail, just like the robustness based methods, on images downsampled by kernels out of their training distribution.

Blind SR-Kernel Estimation: Acknowledging the importance of an accurate SR-kernel, some approaches aim to explicitly estimate the unknown SR-kernel directly from the LR image (e.g., [2, 3, 31, 54, 56]). Notably, [31] was the first to observe that the optimal SR-kernel is the one that maximizes the similarity of small patches *across* different scales of the LR image, and accordingly used cross-scale patch nearest-neighbors to estimate the SR-kernel. KernelGAN [3] further used this principle within deep learning, showing that the SR-kernel can be estimated by training an image-specific GAN on the LR image. However, the zero-shot methods of [3, 31] are pure kernel estimation methods, and require a separate followup algorithm to perform the

SR step on the LR image (e.g., using ZSSR [39] or SRMD [57]), which can receive also a user-specified kernel as an input. This restricts their applicability. Moreover, the explicit kernel estimation methods of [2, 3, 54, 56] can only recover well specific types of kernels (Gaussians and motion lines – see examples in Fig. 1).

Diffusion Models and Inverse Problems: Diffusion probabilistic models [11, 42] have become a powerful tool for modeling complex image distributions. More recently, under the Deep Internal Learning regime [8, 9, 37–39, 45] diffusion-based approaches have been adapted for the single-image setting [21, 33, 47]. Additionally, diffusion models have shown promise in solving inverse problems such as deblurring and super-resolution [4, 18]. Recent works further enhance these approaches by incorporating data-consistency constraints via null-space projections [49] or by adding back-projection steps [15]. These techniques enable zero-shot restoration without retraining, and they demonstrate that iterative diffusion-based refinement can recover high-quality images under unknown degradations. Additional work on patch-based diffusion models [12, 13] further exploits local image statistics for improved detail recovery. Due to their stochastic nature, diffusion models often struggle to strictly adhere to measurement constraints. Moreover, pretrained diffusion models may exhibit a distribution mismatch between the training data and the observed

measurements, necessitating careful adaptation [13].

3. The Importance of an Accurate SR-Kernel

The accuracy of the SR-kernel is critical for achieving high-fidelity HR image reconstruction, often playing a more crucial role than the image prior or SR method itself [7, 22]. The SR process fundamentally relies on inverting the degradation introduced by downsampling, which is dictated by the underlying blur kernel. If the kernel is inaccurate or out of distribution, even advanced SR models risk amplifying artifacts and producing unrealistic results.

This property is shown in Fig. 1: Two state-of-the-art algorithms (SwinIR and StableSR), both trained with blind SR degradations, fail to accurately upscale LR images which were downsampled by non-Gaussian kernels. In contrast, simple interpolation leads to remarkably better visual results. We further confirm this observation quantitatively on 2 datasets with hundreds of LR images downsampled by a variety of *non*-gaussian kernels (“Blind144” & “DIV2KFK” – see Sec. 5.1). These results are summarized in Table 1. The table shows that SotA Blind-SR methods perform *worse* than simple bicubic interpolation on non-gaussian kernels (which are outside their training distribution). Moreover, applying more sophisticated interpolation¹ with the ground-truth (GT) kernel provides an additional large improvement by +1bB over SotA Blind-SR methods on such kernels.

Methods	Blind144		DIV2KFK	
	PSNR↑	SSIM↑	PSNR↑	SSIM↑
Bicubic interpolation	24.865	0.637	24.101	0.639
Interpolation with the GT kernel	25.733	0.659	25.057	0.666
SotA: DCLS-SR [28]/ DPSR [58]	24.808	0.633	23.997	0.637

Table 1. SotA Blind-SR methods perform *worse than interpolation* on LR images downsampled by non-gaussian kernels (Blind144 & DIV2KFK are two such Blind-SR datasets - see Sec. 5.1).

4. Method: “KernelFusion” for Blind-SR

Our method builds on the principle that the correct SR kernel is the one that best preserves the image’s patch distribution across scales. In a first step, a patch-based diffusion model is trained on the LR input image, learning its patch distribution. In a second step, we perform super resolution by iteratively improving our HR guess and estimating the SR-kernel during the reverse diffusion process. Fig. 2 provides an overview over our approach.

4.1. Phase 1: Training Patch-Diffusion (PD)

Our patch-diffusion (PD) model aims to learn the patch distribution of the LR input image I_{LR} . As diffusion mod-

¹Interpolation with a kernel is obtained by backprojection [16] with the estimated Pseudo-Inverse [32, 34] of the kernel.

els are excellent distribution learners, we base our model on the standard denoising probabilistic diffusion model (DDPM) [11], predicting velocity v_t as proposed in [36]. We train it to denoise solely the single LR input image noised with various noise magnitudes, according to a standard DDPM schedule. More specifically, the input is a diffused LR input image to random time step $t \in [1, T]$ while the target is the velocity (from which one can easily derive the clean original input image using a closed form):

$$\Psi = \operatorname{argmin}_{\psi} \left\| PD_{\psi}(x_t) - v_t \right\|_2^2, \quad (2)$$

where $x_t = \sqrt{\bar{\alpha}_t} I_{LR} + \sqrt{1 - \bar{\alpha}_t} \epsilon$, $v_t = \sqrt{\bar{\alpha}_t} \epsilon - \sqrt{1 - \bar{\alpha}_t} I_{LR}$, Ψ are the parameters of our PD model, ϵ is a standard normal white noise, $\bar{\alpha}_t$ is the standard DDPM coefficient.

Learning the patch distribution of a single image requires some adjustments: We took inspiration from [33] using pure CNN without any global layers (such as attention). However, since our method is based on much smaller patches, the receptive field needs to be restricted even further. Thus we exchange the backbone with a simple convolutional network with no strides, introducing a receptive field of 15×15 pixels. This allows training PD on random 64×64 image crops. Further design choices and implementation details can be found in Sec. 4.4.

4.2. Phase 2: Reverse Diffusion at High Resolution

Once PD is trained, it has learned the patch distribution of the LR input image. Next, we perform *simultaneous* SR and kernel estimation, based on the reversed sampling process of PD. This constraints the produced HR image to have the same patch distribution as I_{LR} (which it should have [31]). This combined approach has a major benefit: A better HR prediction \hat{x}_0 leads to an improved kernel prediction, and vice versa. Algorithm 1 provides pseudo-code of the approach, which is further detailed below.

Our method takes as an initial input a bicubically upsampled version of the LR image I_{LR} . This bicubic guess is noised by T_{nd} steps using the diffusion noise schedule. Subsequently, we would like to optimize x_0 at each timestep t , such that the downsampled version $\hat{x}_0 \downarrow_s$ is consistent with the input image I_{LR} . Instead of directly optimizing x_0 , we chose to implicitly optimize x_0 via a U-Net (see Fig. 2). The DIP U-Net [45] imposes a *global* image prior on the output. The PD step used to predict \hat{x}_0 alone does not inherently preserve global structure, especially at high t , due to the 15×15 local receptive field of PD. We solve this problem by applying a DIP U-Net twice: First, we apply the U-Net to x_0 from the previous timestep $t+1$ and reconstruct the required x_t from it. Second, we apply the U-Net after denoising x_t using our patch-diffusion model PD_{ψ} to the predicted x_0 at timestep t . Optimizing the U-Net using our LR consistency loss is hence key to maintain global structure. This setup enables joint training of both the DIP UNET and the kernel

Algorithm 1 Reverse Diffusion Process in KernelFusion

Require:

- Pretrained velocity prediction model: PD_ψ
- Number of noise/denoise timesteps: T_{nd}
- Noise schedule: $\{\beta_t\}_{t=1}^T$ with $\alpha_t = 1 - \beta_t$
- Initial noised bicubic guess:
 $x_{T_{nd}} = \sqrt{\bar{\alpha}_{T_{nd}}}(I_{LR} \uparrow_{bic,s}) + \sqrt{1 - \bar{\alpha}_{T_{nd}}}\epsilon$
with $\epsilon \sim \mathcal{N}(0, I)$
- U-Net network: R_θ
- SIREN network: INR_ϕ
- Kernel coordinate grid: g
- Number of optimization steps per t : n_{iter}
- Learning rate: γ

Ensure: Generated sample x_0 .

```
1: for  $t = T_{nd}$  to 1 do
2:    $\xi \sim \mathcal{N}(0, I)$  ▷ Sample noise
3:   for  $i = 1$  to  $n_{iter}$  do
4:      $\hat{k}_\phi = INR_\phi(g)$  ▷ get kernel
5:      $\hat{x}_{0,t+1,\theta} = R_\theta(x_{0,t+1})$  ▷ get optimized  $x_0$ 
6:      $\hat{x}_t = \mu_{t+1}(\hat{x}_{0,t+1,\theta}, x_{t+1}) + \sigma_{t+1}\xi$ 
7:      $\hat{v}_\theta = PD_\psi(\hat{x}_{t,\theta}, t)$  ▷ denoising step
8:      $\hat{x}_{0,t} = \sqrt{\bar{\alpha}_t} \cdot \hat{x}_{t,\theta} - \sqrt{1 - \bar{\alpha}_t} \cdot \hat{v}_\theta$ 
9:      $\hat{x}_{0,t,\theta} = R_\theta(\hat{x}_{0,t})$  ▷ get optimized  $x_0$ 
10:     $\hat{x}_{0,t} \downarrow_s = (\hat{x}_{0,t} * \hat{k}_\phi) \downarrow_s$  ▷ Downscale step
11:     $\hat{x}_{0,t+1} \downarrow_s = (\hat{x}_{0,t+1} * \hat{k}_\phi) \downarrow_s$  ▷ Downscale step
12:     $\mathcal{L} = \|I_{LR} - \hat{x}_{0,t} \downarrow_s\|_2^2 + \|I_{LR} - \hat{x}_{0,t+1} \downarrow_s\|_2^2$ 
        +  $COM(\hat{k}_\phi)$ 
13:     $\theta = \theta - \gamma \nabla_\theta(\mathcal{L})$  ▷ Step for U-Net
14:     $\phi = \phi - \gamma \nabla_\phi(\mathcal{L})$  ▷ Step for INR
15:  end for
16:   $\mu_t = \beta_t \frac{\bar{\alpha}_{t-1}}{1 - \bar{\alpha}_t} \hat{x}_{0,\theta,\psi} + (1 - \bar{\alpha}_{t-1}) \frac{\alpha_t}{1 - \bar{\alpha}_t} \hat{x}_{t,\theta}$ 
17:   $\zeta \sim \mathcal{N}(0, I)$  ▷ Sample noise
18:   $x_{t-1} = \mu_t + \sigma_t \zeta$  ▷ Add stochasticity,  $\sigma_0 = 0$ 
19: end for
20: return  $x_0$ 
```

estimation network (see Sec. 4.3) with a single loss. Since both networks are trained from scratch, we apply n_{iter} gradient steps at each timestep t . The networks are iteratively refined at every t , leveraging their gradual improvements to enhance the prediction of \hat{x}_0 .

4.3. Kernel Estimation using INR

Estimating a SR-kernel means solving for k_s in Eq. (1). Instead of directly solving for k_s , we chose to represent the kernel via an Implicit Neural Representation (INR) network, which allows us to represent the kernel *continuously* [40], while controlling its level of regularization. Specifically, we took inspiration by the SIREN architecture [41] which is known for its ability to also represent high frequency functions. Specifically, the sinusoidal ac-

tivations enable the network to capture fine-grained structures without introducing over-smoothing, which is critical for accurately estimating complex downscaling kernels k_s .

4.4. Implementation Details

PD Architecture To ensure a small receptive field, we chose to exchange the global-receptive-field U-net of the original DDPM architecture with small, fully convolutional neural network. We use one block consisting of two 3×3 convolutions, followed by six blocks $3 \times 3 + 1 \times 1$ convolutions. This results in a theoretical receptive field of 15×15 pixels. The diffusion model is trained with $T=1000$ time steps. Further implementation details are found in the supplementary material (Sec. A1).

5. Results

5.1. Datasets

We evaluate our method on a variety of blind SR datasets:

DIV2KRRK [3]: From DIV2K [1] validation set (100 images). LR samples are obtained by downscaling each image with a different random gaussian kernel, hence containing anisotropic Gaussians of varying sizes and orientations.

DIV2KFK: Inspired by DIV2KRRK, we created a new dataset based on the 8 real-life downscaling kernels measured by Levin [22], which were induced by small camera jitter during the shutter exposure time. We call this dataset DIV2KFK (DIV2K-Fancy-Kernels). In order to have reasonable blur levels for 4x SR, we resize the original kernels to size 24×24 . Each image of the DIV2K validation set is convolved with a randomly selected kernel and then subsampled by a scale factor of 4.

Blind144: Two factors affect the Blind-SR challenge: the image and the downscaling kernel. To further analyze and better understand SR results, we created the controlled Blind144 dataset. It is organized as a 12×12 matrix comprising 12 images and 12 kernels. This setup allows us to examine the results of a single kernel across various images, as well as the outcomes of a single image across different kernels, thereby clarifying whether specific effects and behaviors stem from the image or the kernel. The images used are the first 12 images from DIV2K. For the selection of kernels we used the 8 empirical kernels as in DIV2KFK, and in addition 3 extreme stress-testing kernels and one anisotropic Gaussian. The purpose of the Gaussian kernel is to compare quality of results on the same image for in-distribution vs. out-of-distribution kernels. The 3 extreme kernels contain an "L" shaped kernel, a full square with sharp edges, and an empty square. These allow stress-testing of kernel extraction. The full set of kernels is displayed in the top row of Fig. 5.



Figure 3. **Blind-SR comparison** on the DIV2KFK dataset (4× upscaling). Each row corresponds to a different degraded image from DIV2KFK, while each column shows the output of a different method at a 4× upscaling factor. Notably, our method reduces doubling artifacts in structured patterns (e.g., aerial road scene, 4th row), demonstrating its effectiveness in restoring fine details and mitigating motion effects.

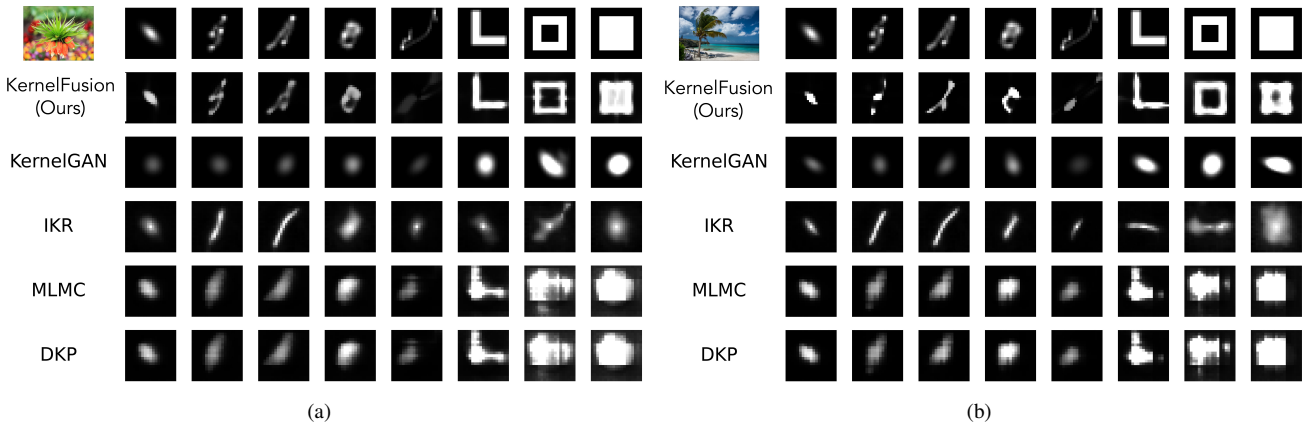


Figure 4. **Comparison of estimated kernels from different Blind-SR methods.** The top row represents the ground-truth (GT) degradation kernels, while each subsequent row corresponds to the estimated kernels from different SR methods, including our approach, KernelGAN, IKR, MLMC, and DKP. Our method demonstrates superior flexibility in recovering complex, non-Gaussian degradations, accurately capturing kernel structures across a diverse range of degradations.

5.2. Empirical Evaluation of SR

We evaluate the quality of the recovered HR images using peak signal-to-noise ratio (PSNR) and structural similarity index measurement (SSIM) [51], with respect to the GT HR images. We orient our evaluation on the procedure of [19]: The evaluation is executed on the luminance chan-

nel (YCBCR space). An image boundary of $\sim 5\%$ is excluded in the PSNR/SSIM estimation, due to boundary effects.

Table 2 compares KernelFusion with a variety of SotA competitors. Our method surpasses all SotA blind-SR methods by a large margin on both DIV2KFK and Blind144, and delivers comparable results on the

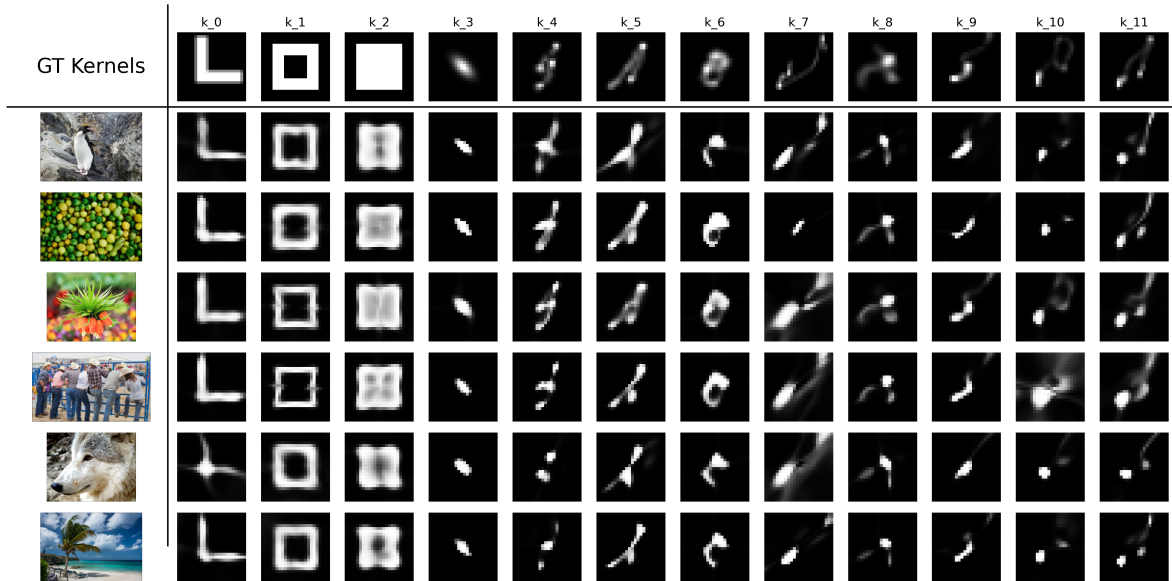


Figure 5. **Kernel estimation results on Blind144.** The top row displays the 12 ground-truth (GT) degradation kernels, including real-world motion blur kernels from [22], an anisotropic Gaussian kernel, and three synthetic non-natural kernels (L-shape, empty square, and filled square). The subsequent rows show our method’s estimated kernels for each of the 12 kernels applied to the first 12 images of the DIV2K validation set. Our approach successfully captures a diverse range of degradations, including complex structured kernels, demonstrating its robustness and adaptability in blind SR kernel estimation.

Dataset	Metric	Bicubic interpolation	SinSR [50]	StableSR [46]	SwinIR [24]	DPSR [58]	IKR [2]	RealDAN [29]	RealDAN GAN	RealDAN specialized	DCLS-SR [28] ²	DiffBIR [26]	DKP [56]	MLMC [54]	KernelGAN +ZSSR [3]	KernelFusion (ours)
Blind144	PSNR↑	<u>24.865</u>	23.587	23.775	23.773	24.824	24.113	24.624	23.998	-	24.808	24.259	23.431	23.430	24.529	27.058
	SSIM↑	0.637	0.582	0.625	0.616	0.637	0.630	<u>0.638</u>	0.619	-	0.633	0.599	0.612	0.612	0.633	0.715
DIV2KRK	PSNR↑	25.075	25.360	25.262	25.139	25.317	23.906	26.870	26.057	27.821	<u>27.150</u>	25.431	23.127	23.122	25.895	26.747
	SSIM↑	0.671	0.680	0.709	0.699	0.682	0.667	0.745	0.730	0.775	<u>0.748</u>	0.668	0.629	0.629	0.703	0.714
DIV2KFK	PSNR↑	<u>24.101</u>	22.887	23.077	23.070	23.977	23.352	23.941	23.439	-	23.886	23.546	22.531	22.535	23.617	26.155
	SSIM↑	0.639	0.585	0.630	0.620	0.637	0.627	<u>0.644</u>	0.628	-	0.634	0.606	0.603	0.604	0.629	0.711

Table 2. **Quantitative comparison of methods on 4x SR across different Blind-SR datasets.** The 2 best results per dataset (row) are highlighted in **bold** and underline. Note that on the 2 non-gaussian datasets (DIV2KFK and Blind144), KernelFusion is best (by a large margin), and Bicubic interpolation is second. (Comments: (i) “RealDAN specialized” is a version of “RealDAN” specialized for Gaussian kernels only, hence applied only to DIV2KRK. (ii) The reported PSNRs are after excluding an image boundary of 5%, due to boundary effects.)

DIV2KRK dataset. It is worth noting that a simple bicubic upscaling surpasses all SotA methods in PSNR on DIV2KFK & Blind144, indicating that these methods completely fail adapting to out-of-distribution downscaling.

Fig. 3 showcases SR results on the DIV2KFK dataset, comparing our method against SotA approaches. Our method demonstrates superior reconstruction quality, particularly in challenging regions such as text, structured patterns, and natural textures. Notably, in Fig. 1, row 1, which contains the State Bank of Mysore sign, most competing methods struggle to recover clear and legible text, often introducing excessive blurring or ghosting artifacts, whereas our method produces sharper, more readable characters. A similar trend is observed in the aerial road scene (Fig. 3, row 4), where other methods introduce noticeable doubling artifacts (misaligned white car), which are significantly re-

duced in our results. Furthermore, our approach maintains a balance between sharpness and natural texture preservation in human faces and complex textures, avoiding the over-sharpening and aliasing effects present in some models (e.g., RealDAN and DIFFBIR). These results demonstrate the robustness of our approach in handling diverse realistic motion degradations present in the DIV2KFK dataset.

5.3. Kernel Evaluation

To assess the effectiveness of different blind-SR methods in kernel estimation, we visualize the predicted SR-kernels in Fig. 4. The top row represents the ground-truth (GT) kernels, while subsequent rows correspond to the estimated kernels from various blind-SR methods that explicitly estimate the SR-kernel (including ours). KernelGAN demonstrates a strong bias toward Gaussian-like kernels, failing to

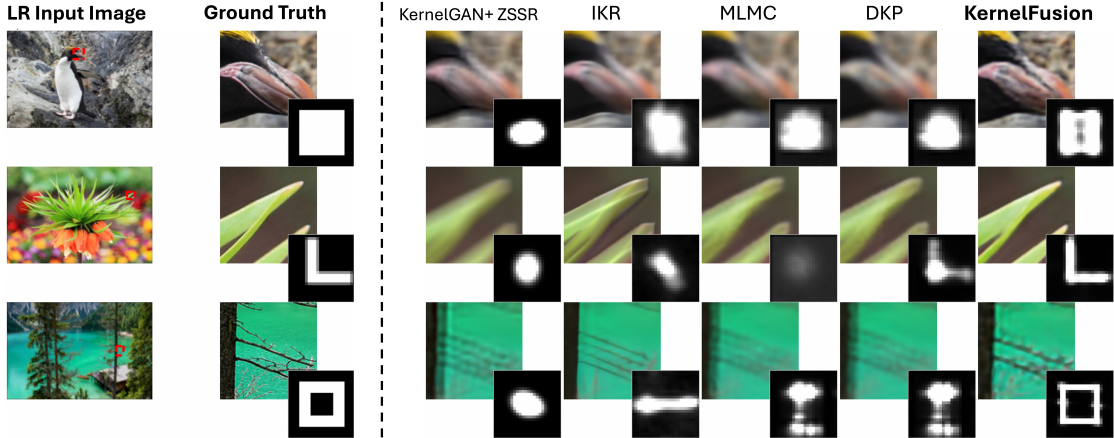


Figure 6. Additional examples of explicit kernel recovery and SR under extreme downscaling kernels.

accurately capture non-Gaussian degradations. IKR, which was trained with a mixture of random Gaussian and motion blur kernels, exhibits improved performance on motion kernels but struggles to generalize beyond its training distribution, often producing elongated blur patterns. Both MLMC and DKP leverage meta-learning and Markov Chain Monte Carlo (MCMC) simulations to infer kernel priors without explicit assumptions. As a result, they are more flexible in capturing diverse degradation patterns. However, despite their adaptive nature, their estimated kernels still exhibit noticeable deviations from the GT, particularly in the case of extreme degradations. Unlike prior methods, our approach does not impose any priors on the kernel shape, allowing it to accurately recover challenging degradations. Fig. 5 presents our estimated kernels across samples from the Blind144. As observed, our approach is capable of recovering a diverse range of kernel structures, demonstrating the flexibility of our kernel estimation process. The entire collection of 144 kernels recovered by KernelFusion from the Blind144 dataset can be found in Fig. S1 in the Supplementary. Additionally, Fig. 6 shows some more SR and kernel extraction comparison for extreme kernels.

6. Limitations

KernelFusion currently accounts for super-resolving LR images obtained under severe *downscaling* degradations, which were previously considered impossible. However, while it can handle mild noise in the LR image, KernelFusion is currently not catered to handle other types of *severe* degradations (like strong JPEG artifacts, or severe noise in the LR image). This is because the Patch-Diffusion competent aims to preserve the same patch statistics in the recovered HR image as in the LR input image (and would therefore include also severe noise and/or JPEG artifacts). Extending KernelFusion to handle other types of degrada-

tions *in a blind manner* is part of our future work.

Additionally, our method relies solely on the internal statistics of a single image (the LR image), without leveraging any external priors or pre-trained large-scale diffusion models. Although this assumption-free design is central to our ability to tackle previously intractable downscaling degradations, it does not exploit rich external information which could enhance reconstruction quality. Moreover, patch diffusion has to be trained from scratch on each new LR image, taking ~ 20 minutes per image. The following upscaling process then depends on input image size and scale factor applied. Exploring approaches to integrate *external* learned priors with our *internal* Patch-Diffusion model may significantly speed up KernelFusion, as well as potentially improve its output quality. This represents an exciting direction for future research.

7. Conclusion

“KernelFusion” recovers the unique image-specific SR-kernel directly from the LR input image, while simultaneously recovering its corresponding HR image in a consistent manner. It can handle complex downscaling degradations, where existing SotA Blind-SR methods fail miserably. Being a zero-shot estimation method which trains *internally* on the LR input image only, KernelFusion is not bound by any external training distribution, hence can handle any type of downscaling kernel. It has no notion of “out-of-distribution” kernels, which *externally-trained* Blind-SR methods suffer from. By breaking free from predefined kernel assumptions, KernelFusion pushes Blind-SR into a new, assumption-free paradigm — handling downscaling degradations previously thought impossible.

References

- [1] Eirikur Agustsson and Radu Timofte. Ntire 2017 challenge on single image super-resolution: Dataset and study. In *Proceedings of the IEEE conference on computer vision and pattern recognition workshops*, pages 126–135, 2017. 5
- [2] Hasan F Ates, Suleyman Yildirim, and Bahadir K Gunturk. Deep learning-based blind image super-resolution with iterative kernel reconstruction and noise estimation. *Computer Vision and Image Understanding*, 233:103718, 2023. 2, 3, 7
- [3] Sefi Bell-Kligler, Assaf Shocher, and Michal Irani. Blind super-resolution kernel estimation using an internal-gan. *Advances in neural information processing systems*, 32, 2019. 2, 3, 5, 7
- [4] Hyungjin Chung, Jiaming Song, and Stefano Ermon. Diffusion posterior sampling for general noisy inverse problems. In *NeurIPS*, 2022. 3
- [5] Marcos V Conde, Ui-Jin Choi, Maxime Burchi, and Radu Timofte. Swin2sr: Swin2 transformer for compressed image super-resolution and restoration. In *European Conference on Computer Vision*, pages 669–687. Springer, 2022. 2
- [6] Chao Dong, Chen Change Loy, Kaiming He, and Xiaoou Tang. Image super-resolution using deep convolutional networks. *IEEE transactions on pattern analysis and machine intelligence*, 38(2):295–307, 2015. 2
- [7] Netalee Efrat, Daniel Glasner, Alexander Apartsin, Boaz Nadler, and Anat Levin. Accurate blur models vs. image priors in single image super-resolution. In *Proceedings of the IEEE International Conference on Computer Vision*, pages 2832–2839, 2013. 2, 4
- [8] Yosef Gandelsman, Assaf Shocher, and Michal Irani. ”double-dip”: unsupervised image decomposition via coupled deep-image-priors. In *Proceedings of the IEEE/CVF conference on computer vision and pattern recognition*, pages 11026–11035, 2019. 3
- [9] Niv Granot, Ben Feinstein, Assaf Shocher, Shai Bagon, and Michal Irani. Drop the gan: In defense of patches nearest neighbors as single image generative models. In *Proceedings of the IEEE/CVF conference on computer vision and pattern recognition*, pages 13460–13469, 2022. 3
- [10] Jinjin Gu, Hannan Lu, Wangmeng Zuo, and Chao Dong. Blind super-resolution with iterative kernel correction. In *CVPR*, 2019. 2, 3
- [11] Jonathan Ho, Ajay Jain, and Pieter Abbeel. Denoising diffusion probabilistic models. *Advances in neural information processing systems*, 33:6840–6851, 2020. 3, 4
- [12] Jason Hu, Bowen Song, Jeffrey Fessler, and Liyue Shen. Patch-based diffusion models beat whole-image models for mismatched distribution inverse problems. 2024. 3
- [13] Jason Hu, Bowen Song, Xiaojian Xu, Liyue Shen, and Jeffrey Fessler. Learning image priors through patch-based diffusion models for solving inverse problems. In *NeurIPS*, 2024. 3, 4
- [14] Yan Huang, Shang Li, Wen He, Liang Wang, and Tieniu Tan. Unfolding the alternating optimization for blind super-resolution. In *NeurIPS*, 2020. 2, 3
- [15] Zheng Hui, Kai Wang, Jiaming Yang, and Xinbo Gao. Accelerating diffusion models for inverse problems through short-cut sampling. In *IJCAI*, 2024. 3
- [16] Michal Irani and Shmuel Peleg. Improving resolution by image registration. *CVGIP: Graphical models and image processing*, 53(3):231–239, 1991. 4
- [17] Younghyun Jo, Seoung Wug Oh, Peter Vajda, and Seon Joo Kim. Tackling the ill-posedness of super-resolution through adaptive target generation. In *CVPR*, 2021. 2
- [18] Bahjat Kawar, Michael Elad, Stefano Ermon, and Jiaming Song. Denoising diffusion restoration models. *Advances in Neural Information Processing Systems*, 35:23593–23606, 2022. 3
- [19] Jiwon Kim, Jung Kwon Lee, and Kyoung Mu Lee. Accurate image super-resolution using very deep convolutional networks. In *Proceedings of the IEEE conference on computer vision and pattern recognition*, pages 1646–1654, 2016. 2, 6
- [20] Soo Ye Kim, Hyeonjun Sim, and Munchurl Kim. Koalanet: Blind super-resolution using kernel-oriented adaptive local adjustment. In *CVPR*, 2021. 2, 3
- [21] Matan Kleiner, Vladimir Kulikov, Shahar Yadin, and Tomer Michaeli. SinDDM: Single image denoising diffusion model. In *ICML*, 2023. 3
- [22] Anat Levin, Yair Weiss, Fredo Durand, and William T Freeman. Understanding and evaluating blind deconvolution algorithms. In *2009 IEEE conference on computer vision and pattern recognition*, pages 1964–1971. IEEE, 2009. 2, 4, 5, 7
- [23] Feng Li, Yixuan Wu, Zichao Liang, Runmin Cong, Huihui Bai, Yao Zhao, and Meng Wang. Blinddiff: Empowering degradation modelling in diffusion models for blind image super-resolution. *arXiv preprint arXiv:2403.10211*, 2024. 2
- [24] Jingyun Liang, Jiezhong Cao, Guolei Sun, Kai Zhang, Luc Van Gool, and Radu Timofte. Swinir: Image restoration using swin transformer. In *Proceedings of the IEEE/CVF international conference on computer vision*, pages 1833–1844, 2021. 2, 7
- [25] Bee Lim, Sanghyun Son, Heewon Kim, Seungjun Nah, and Kyoung Mu Lee. Enhanced deep residual networks for single image super-resolution. In *Proceedings of the IEEE conference on computer vision and pattern recognition workshops*, pages 136–144, 2017. 2
- [26] Xinqi Lin, Jingwen He, Ziyang Chen, Zhaoyang Lyu, Bo Dai, Fanghua Yu, Yu Qiao, Wanli Ouyang, and Chao Dong. Diffbir: Toward blind image restoration with generative diffusion prior. In *European Conference on Computer Vision*, pages 430–448. Springer, 2024. 2, 7
- [27] Anran Liu, Yihao Liu, Jinjin Gu, Yu Qiao, and Chao Dong. Blind image super-resolution: A survey and beyond. *IEEE transactions on pattern analysis and machine intelligence*, 45(5):5461–5480, 2022. 2
- [28] Ziwei Luo, Haibin Huang, Lei Yu, Youwei Li, Haoqiang Fan, and Shuaicheng Liu. Deep constrained least squares for blind image super-resolution. In *CVPR*, 2022. 2, 3, 4, 7
- [29] Zhengxiong Luo, Yan Huang, Shang Li, Liang Wang, and Tieniu Tan. End-to-end alternating optimization for real-world blind super resolution. *International Journal of Computer Vision*, 131(12):3152–3169, 2023. 2, 3, 7

- [30] Ziwei Luo, Haibin Huang, Lei Yu, Youwei Li, Bing Zeng, and Shuaicheng Liu. Kernel reformulation with deep constrained least squares for blind image super-resolution. *IEEE Transactions on Circuits and Systems for Video Technology*, 2025. 2
- [31] Tomer Michaeli and Michal Irani. Nonparametric blind super-resolution. In *Proceedings of the IEEE International Conference on Computer Vision*, pages 945–952, 2013. 2, 3, 4
- [32] E.H. Moore. The fourteenth western meeting of the american mathematical society, 1920. 4
- [33] Yaniv Nikankin, Niv Haim, and Michal Irani. Sinfusion: Training diffusion models on a single image or video. In *ICML*, 2023. 3, 4
- [34] R. Penrose. A generalized inverse for matrices. *Mathematical Proceedings of the Cambridge Philosophical Society*, 51(3):406–413, 1955. 4
- [35] Chitwan Saharia, Jonathan Ho, William Chan, Tim Salimans, David J Fleet, and Mohammad Norouzi. Image super-resolution via iterative refinement. *IEEE transactions on pattern analysis and machine intelligence*, 45(4):4713–4726, 2022. 2
- [36] Tim Salimans and Jonathan Ho. Progressive distillation for fast sampling of diffusion models. *arXiv preprint arXiv:2202.00512*, 2022. 4
- [37] Tamar Rott Shaham, Tali Dekel, and Tomer Michaeli. Singan: Learning a generative model from a single natural image. In *Proceedings of the IEEE/CVF international conference on computer vision*, pages 4570–4580, 2019. 3
- [38] Assaf Shocher, Shai Bagon, Phillip Isola, and Michal Irani. Ingan: Capturing and remapping the” dna” of a natural image. *arXiv preprint arXiv:1812.00231*, 2018.
- [39] Assaf Shocher, Nadav Cohen, and Michal Irani. Zero-shot super-resolution using deep internal learning. In *CVPR*, 2018. 2, 3
- [40] Assaf Shocher, Ben Feinsein, Niv Haim, and Michal Irani. From discrete to continuous convolution layers. *arXiv preprint arXiv:2006.11120*, 2020. 5
- [41] Vincent Sitzmann, Julien Martel, Alexander Bergman, David Lindell, and Gordon Wetzstein. Implicit neural representations with periodic activation functions. *Advances in neural information processing systems*, 33:7462–7473, 2020. 5, 13
- [42] Jascha Sohl-Dickstein, Eric Weiss, Niru Maheswaranathan, and Surya Ganguli. Deep unsupervised learning using nonequilibrium thermodynamics. In *International conference on machine learning*, pages 2256–2265. pmlr, 2015. 3
- [43] Xiaopeng Sun, Qinwei Lin, Yu Gao, Yujie Zhong, Chengjian Feng, Dengjie Li, Zheng Zhao, Jie Hu, and Lin Ma. Rfsr: Improving isr diffusion models via reward feedback learning. *arXiv preprint arXiv:2412.03268*, 2024. 2
- [44] Matthew Tancik, Pratul Srinivasan, Ben Mildenhall, Sara Fridovich-Keil, Nithin Raghavan, Utkarsh Singhal, Ravi Ramamoorthi, Jonathan Barron, and Ren Ng. Fourier features let networks learn high frequency functions in low dimensional domains. *Advances in neural information processing systems*, 33:7537–7547, 2020. 2
- [45] Dmitry Ulyanov, Andrea Vedaldi, and Victor Lempitsky. Deep image prior. In *Proceedings of the IEEE conference on computer vision and pattern recognition*, pages 9446–9454, 2018. 3, 4
- [46] Jianyi Wang, Zongsheng Yue, Shangchen Zhou, Kelvin CK Chan, and Chen Change Loy. Exploiting diffusion prior for real-world image super-resolution. *International Journal of Computer Vision*, 132(12):5929–5949, 2024. 2, 7
- [47] Weilun Wang, Jianmin Bao, Wengang Zhou, Dongdong Chen, Dong Chen, Lu Yuan, and Houqiang Li. SinDiffusion: Learning a diffusion model from a single natural image. *arXiv:2211.12445*, 2022. 3
- [48] Xintao Wang, Liangbin Xie, Chao Dong, and Ying Shan. Real-esrgan: Training real-world blind super-resolution with pure synthetic data. In *arXiv:2107.10833*, 2021. 2
- [49] Yinhuai Wang, Jiwen Yu, and Jian Zhang. Zero-shot image restoration using denoising diffusion null-space model. In *ICLR*, 2023. 3
- [50] Yufei Wang, Wenhan Yang, Xinyuan Chen, Yaohui Wang, Lanqing Guo, Lap-Pui Chau, Ziwei Liu, Yu Qiao, Alex C Kot, and Bihan Wen. Sinsr: diffusion-based image super-resolution in a single step. In *Proceedings of the IEEE/CVF Conference on Computer Vision and Pattern Recognition*, pages 25796–25805, 2024. 2, 7
- [51] Zhou Wang, Alan C Bovik, Hamid R Sheikh, and Eero P Simoncelli. Image quality assessment: from error visibility to structural similarity. *IEEE transactions on image processing*, 13(4):600–612, 2004. 6
- [52] Pengxu Wei, Ziwei Xie, Hannan Lu, Zongyuan Zhan, Qixiang Ye, Wangmeng Zuo, and Liang Lin. Component divide-and-conquer for real-world image super-resolution. In *Computer Vision—ECCV 2020: 16th European Conference, Glasgow, UK, August 23–28, 2020, Proceedings, Part VIII 16*, pages 101–117. Springer, 2020. 2
- [53] Rongyuan Wu, Tao Yang, Lingchen Sun, Zhengqiang Zhang, Shuai Li, and Lei Zhang. Seesr: Towards semantics-aware real-world image super-resolution. In *Proceedings of the IEEE/CVF conference on computer vision and pattern recognition*, pages 25456–25467, 2024. 2
- [54] Jingyuan Xia, Zhixiong Yang, Shengxi Li, Shuanghui Zhang, Yaowen Fu, Deniz Gündüz, and Xiang Li. Blind super-resolution via meta-learning and markov chain monte carlo simulation. *IEEE Transactions on Pattern Analysis and Machine Intelligence*, 2024. 2, 3, 7
- [55] Tao Yang, Rongyuan Wu, Peiran Ren, Xuansong Xie, and Lei Zhang. Pixel-aware stable diffusion for realistic image super-resolution and personalized stylization. In *European Conference on Computer Vision*, pages 74–91. Springer, 2024. 2
- [56] Zhixiong Yang, Jingyuan Xia, Shengxi Li, Xinghua Huang, Shuanghui Zhang, Zhen Liu, Yaowen Fu, and Yongxiang Liu. A dynamic kernel prior model for unsupervised blind image super-resolution. In *Proceedings of the IEEE/CVF conference on computer vision and pattern recognition*, pages 26046–26056, 2024. 2, 3, 7
- [57] Kai Zhang, Wangmeng Zuo, Shuhang Gu, and Lei Zhang. Learning a single convolutional super-resolution network for multiple degradations. In *CVPR*, 2018. 2, 3

- [58] Kai Zhang, Wangmeng Zuo, and Lei Zhang. Deep plug-and-play super-resolution for arbitrary blur kernels. In *Proceedings of the IEEE/CVF conference on computer vision and pattern recognition*, pages 1671–1681, 2019. [4](#), [7](#)
- [59] Kai Zhang, Wing Lau, and Chen Change Loy. Deep unfolding network for image super-resolution. In *CVPR*, 2020. [3](#)
- [60] Kai Zhang, Jingyun Liang, Luc Van Gool, and Radu Timofte. Designing a practical degradation model for deep blind image super-resolution. In *ICCV*, 2021. [2](#)
- [61] Wenlong Zhang, Xiaohui Li, Guangyuan Shi, Xiangyu Chen, Yu Qiao, Xiaoyun Zhang, Xiao-Ming Wu, and Chao Dong. Real-world image super-resolution as multi-task learning. *Advances in Neural Information Processing Systems*, 36, 2024. [2](#)
- [62] Yulun Zhang, Kunpeng Li, Kai Li, Lichen Wang, Bineng Zhong, and Yun Fu. Image super-resolution using very deep residual channel attention networks. In *ECCV*, 2018. [2](#)
- [63] Yulun Zhang, Yapeng Tian, Yu Kong, Bineng Zhong, and Yun Fu. Residual dense network for image super-resolution. In *Proceedings of the IEEE conference on computer vision and pattern recognition*, pages 2472–2481, 2018. [2](#)

Supplementary Material



Figure S1. **Estimated kernels of KernelFusion on Blind144:** Complete overview of all 144 estimated kernels.

A1. Further Technical Details

A1.1. Patch-Diffusion

Architecture The backbone model is a convolutional network, that inputs an image tensor x and a timestep t . We have a total of 6 blocks, each block conditioned on t . We use one block of two 3×3 filters, followed by six blocks of $3 \times 3 + 1 \times 1$ filters. We use 128 filters for the hidden layers.

Training Details The patch diffusion model is trained using random crops of size 64 pixels. The model is trained for 600'000 steps, using Adam as optimizer, with a learning rate of $lr = 1 \times 10^{-4}$ and cosine annealing.

A1.2. U-Net

Architecture The refinement UNET consists of 5 blocks, with 32 filters on the input level and 512 filters on the bottom level. Each block consists of 2 convolutional layers with a 3×3 kernel, ReLU activations and batch norm. The final layer uses a tanh activation function to ensure that the predicted x_0 output is in the expected -1 to 1 range. The levels are down respectively upsampled by a scale factor of 2.

Training Details The UNET is trained at each time step t during the reverse diffusion process. We use Adam optimizer, a learning rate of $lr = 1 \times 10^{-4}$. We apply cosine annealing, reducing the learning rate at each t to $lr = 5 \times 10^{-5}$. The UNET is initialized at the first T_{start} of the reverse diffusion process and then finetuned along the different timesteps t . With the exception of the initial T_{start} where we apply 100 iterations, the model is then finetune for 20 iterations during each t .

A1.3. Implicit Neural Representation for Kernel Estimation

Architecture As described in Sec. 4.3, we took inspiration from SIREN [41] for our implicit neural representation. The network consists of 5 fully connected layers, with 256 nodes each. In contrast to the original paper, we reduced ω from 30 to 5 and apply it across all layers. Our last layer has an activation function which we call *leaky sigmoid*, a sigmoid function also allowing for slight negative values: $\sigma_{leaky}(x) = (1 + 10^{-4}) \cdot \sigma(x) - 10^{-4}$.

Training Details As we train our INR along with the UNET, we use the same training setup as described in Sec. A1.2.